Draft version November 12, 2021
Typeset using LaTeX **twocolumn** style in AASTeX631

# Searching for TESS Photometric Variability of Possible JWST Spectrophotometric Standard Stars

Susan E. Mullally [1], G. C. Sloan [1,2], J. J. Hermes [3], Michael Kunz [1,4], Kelly Hambleton [5], Ralph Bohlin [1], Scott W. Fleming [1], Karl D. Gordon [1], Catherine Kaleida [1], and Khalid Mohamed [1,6]

[1] *Space Telescope Science Institute, 3700 San Martin Dr., Baltimore, MD 21218, USA*
[2] *Department of Physics and Astronomy, University of North Carolina, Chapel Hill, NC 27599-3255, USA*
[3] *Department of Astronomy & Institute for Astrophysical Research, Boston University, 725 Commonwealth Ave., Boston, MA 02215, USA*
[4] *Albert Einstein High School, Kensington, MD, 20895*
[5] *Villanova University, 800 Lancaster Avenue, Villanova, PA 19850, USA*
[6] *Department of Physics & Astronomy, Amherst College, C025 Science Center 25 East Drive, Amherst, MA 01002, USA*

## ABSTRACT

We use data from the Transiting Exoplanet Survey Satellite (TESS) to search for, and set limits on, optical to near-infrared photometric variability of the candidate James Webb Space Telescope (JWST) spectrophotometric standards. Our search of 37 of these candidate standards has revealed measurable periodic variability in 15 stars. The majority of those show variability that is less than half a percent; however, four stars are observed to vary photometrically, from minimum to maximum flux, by more than 1% (the G dwarf HD 38949 and three fainter A dwarfs). Variability of this size would likely impact the error budget in the spectrophotometric calibration of the science instruments aboard JWST. For the 22 candidate standards with no detected variability, we report upper limits on the observed changes in flux. Despite some systematic noise, all stars brighter than $12^{th}$ magnitude in the TESS band show a $3\sigma$ upper limit on the total change in brightness of less than half a percent on time scales between an hour and multiple weeks, empirically establishing their suitability as spectrophotometric standards.

*Keywords:* variable stars, white dwarfs, calibration

## 1. INTRODUCTION

The James Webb Space Telescope (JWST), an infrared space telescope with a diameter of 6.5 m, promises to revolutionize many areas of astrophysics, from exoplanets to the most distant galaxies (Kalirai 2018; Gardner et al. 2006). In order to accomplish those goals, JWST will observe a sample of spectrophotometric standard stars to calibrate observations across the near- and mid-infrared (0.6–28.8 $\mu$m). The objective is an accuracy in the observed flux of the standard stars to better than 2% (see JWST Data Absolute Flux Calibration in JWST User Documentation 2016). A successful standard-star calibration program will not only enable the absolute calibration and the JWST cross-instrument calibration, but will also tie JWST observations to other space telescopes, such as Hubble, Spitzer, and WISE, and other ground-based observatories.

smullally@stsci.edu

The selection of standard stars must take into account many factors that can reduce both the accuracy and the precision of the spectrophotometric calibration. The list of possible reasons to reject potential standards during the vetting process is long, but among them, variability is always a red flag. Variable stars should be avoided because their variations will increase the noise in the calibration data. Even low-amplitude variability below any level of direct concern could point to more subtle concerns, such as binarity, pulsation, strong magnetic-field activity, or the presence of circumstellar material (Bohlin et al. 2014). Each of these issues is a reason in itself to reject a candidate, but may have otherwise gone unnoticed. The identification of any known variable stars prior to their observation by JWST will give the calibration team the opportunity to investigate them more closely and potentially save valuable observing time. Optimizing the calibration of JWST will contribute to the success of NASA's flagship mission.

High-cadence photometric surveys of stars, as done by missions like CoRoT (Auvergne et al. 2009), Kepler (Koch et al. 2010) and TESS (Ricker et al. 2015), has revealed that they can change brightness due to a variety of factors, and these variations can unexpectedly change in timescale or amplitude. Many of these variations are internal to the star, e.g. stellar pulsations or spots rotating in and out of view (e.g. Breger 1979; McQuillan et al. 2014), while other variations are external, e.g. eclipses and transits (e.g. Prša et al. 2011; Thompson et al. 2018). Time-series photometric observations have revealed many examples of atypical brightness variations where stars change brightness suddenly and in unexpected ways. For example, Boyajian's star, KIC 8462852, was discovered using Kepler data and shows unexplained drops in the flux of the star as large as 20% at seemingly random times (Boyajian et al. 2016). The nearby red supergiant Betelgeuse dimmed by more than one visual magnitude in 2019, the deepest decline reported in 50-plus years of observations (Montargès et al. 2021; Cotton et al. 2020). Some white dwarf stars, the classic choice for photometric standards in the UV and optical, have shown both unusual intrinsic variability from pulsations (e.g. Provencal et al. 2009; Kilic et al. 2015; Hermes et al. 2017) and external variability caused by accretion disks (Scaringi et al. 2021) or disintegrating planetesimals (as large as 40%; Vanderburg et al. 2015; Guidry et al. 2021). While these examples are rare, they demonstrate that stars can vary for a variety of reasons, many of which are not predictable based on current knowledge.

TESS is well positioned to monitor the candidate standards for JWST for changes in flux on time scales between minutes and weeks at a precision as fine as a few hundred parts per million (Ricker et al. 2015), an improvement in precision, cadence and coverage over previous observations to identify short term variability in standard stars from the ground (e.g., Marinoni et al. 2016). TESS was launched in 2017 with the purpose of identifying transiting exoplanets around nearby stars. It photometrically observes a swath of sky covering 24 degrees by 90 degrees for a month at a time and has a bandpass of 0.6–1 $\mu$m (Ricker et al. 2015) that overlaps with the shortest wavelengths of the JWST bandpass.

As a result, TESS has serendipitously observed most of the candidate spectrophotometric standards for JWST over the course of its mission, and it will continue to do so in its extended mission. We have examined the TESS data for these candidates, looked for evidence of photometric variability, and we report upper limits on any variability if none was detected. For the 15 candidate spectrophotometric standards found to show statistically significant periodic variability, we show a light curve and periodogram, and provide a few basic statistics describing the amplitude of the variations.

## 2. CANDIDATE JWST SPECTROPHOTOMETRIC STANDARD STARS

Spectrophotometric calibration requires accurate models of the stars chosen as standards, because any errors in the assumed true spectrum of a standard will propagate into the entire calibrated database (e.g. Cohen et al. 1992; Price et al. 2002; Sloan et al. 2015). Calibrating with a sample of standards will reduce the impact of problems with the model of any one star, and combining different types of standards will reduce the problems even further. By comparing the calibration as determined from different stars, and different classes of stars, outliers can be identified and their models corrected, or, if that proves impossible, the stars can be rejected.

The JWST calibration will be based on three classes of standard stars: white dwarfs, A dwarfs, and solar analogs (i.e., G dwarfs) (Gordon et al. 2022). It is expected that a minimum of five stars of each class will be observed during the JWST mission to accomplish this task. Comparisons of the stars will identify potential issues with models of the stars and possible outliers. The sample examined in this paper, see Table 1, is based on lists of candidates available in the JWST User Documentation accessed in 2020 December[1] (JWST User Documentation 2016). It must be stressed that the candidate list is evolving as stars are vetted and new stars are added to better cover parameter space (Gordon et al. 2022). The calibration standard stars in this list overlap calibration stars used by other observatories. For example, the list includes A dwarf stars reported by Reach et al. (2005) to be primary standards for IRAC on Spitzer (see those with shortened names starting with J in Table 1). For more information on how the calibration stars are selected, see Gordon et al. (2022).

[1] https://jwst-docs.stsci.edu/jwst-data-calibration-considerations/jwst-data-absolute-flux-calibration

**Table 1**. Candidate standard star properties with TESS data.

| Target Name | TIC ID | Class | T | Cadence | Coord. |
|---|---|---|---|---|---|
| | | | [mag] | min | J2000 |
| GSPC P330-E | 8591766 | G2V | 12.4 | 30 | 16 31 34 +30 08 46 |
| 16 Cyg B | 27533327 | G3V | 5.6 | 2 | 19 41 52 +50 31 03 |
| HD 38949[a] | 32869782 | G1V | 7.3 | 2 | 05 48 20 −24 27 50 |
| HD 6538 | 39464221 | G1V | 5.9 | 2 | 17 32 01 +34 16 16 |
| $\eta^1$ Dor | 41232189 | A0V | 5.8 | 2 | 06 06 09 −66 02 23 |
| $\mu$ Col | 100589904 | O9.5V | 5.5 | 2 | 05 46 00 −32 18 23 |
| 10 Lac | 128692445 | O9V | 5.1 | 2 | 22 39 16 +39 03 01 |
| HD 37962 | 140282069 | G2V | 7.2 | 2 | 05 40 52 −31 21 04 |
| WD 1057+719 | 147921014 | DA1.2 | 15.1 | 2 | 11 00 34 +71 38 03 |
| GD 153 | 149505899 | DA1.2 | 13.7 | 2 | 12 57 02 +22 01 53 |
| HD 116405 | 165370459 | A0V | 8.4 | 2 | 13 22 45 +44 42 54 |
| HR 701 | 166698220 | A5V | 5.7 | 2 | 02 22 55 −51 05 32 |
| HD 101452 | 181240911 | A2/3(m)A8-F2 | 7.3 | 2 | 11 40 14 −39 08 48 |
| HR 6514 | 198456033 | A4V | 6.4 | 2 | 17 26 05 +58 39 07 |
| J1757132* | 219094190 | (A3V) | 11.6 | 30 | 17 57 13 +67 03 41 |
| GSPC P041-C[b] | 219015049 | (G0V) | 11.5 | 2 | 14 51 58 +71 43 17 |
| J1808347* | 219114641 | (A3V) | 11.9 | 2 | 18 08 35 +69 27 29 |
| BD+60 1753 | 219752116 | A1V | 9.7 | 2 | 17 24 52 +60 25 51 |
| HD 163466 | 219820925 | A2 | 6.7 | 2 | 17 52 25 +60 23 47 |
| J1732526* | 219897252 | (A4V) | 12.5 | 2 | 17 32 53 +71 04 43 |
| HD 180609 | 229945862 | (A0V) | 9.3 | 2 | 19 12 47 +64 10 37 |
| HD 115169[c] | 229980646 | G3V | 8.7 | 2 | 13 15 47 −29 30 21 |
| J1802271* | 233067231 | (A2V) | 12.0 | 2 | 18 02 27 +60 43 36 |
| J1805292* | 233075513 | (A4V) | 12.2 | 2 | 18 05 29 +64 27 52 |
| J1812095* | 233095291 | (A3V) | 11.6 | 2 | 18 12 10 +63 29 42 |
| J1743045* | 233205654 | (A5V) | 13.3 | 2 | 17 43 04 +66 55 02 |
| GD 71 | 247923021 | DA0.8 | 13.4 | 2 | 05 52 28 +15 53 13 |
| HR 5467 | 298165335 | A1V | 5.8 | 2 | 14 38 15 +54 01 24 |
| G191-B2B | 327587572 | DA0.8 | 12.2 | 2 | 05 05 31 +52 49 52 |
| HD 167060 | 365653206 | G3V | 8.4 | 2 | 18 17 44 −61 42 32 |
| $\delta$ UMi | 383553764 | A1Van | 4.4 | 2 | 17 32 13 +86 35 11 |
| HR 7018[d] | 383676357 | A0V | 5.8 | 2 | 18 37 34 +62 31 36 |
| GSPC P177-D | 417544924 | (G0) | 12.9 | 30 | 15 59 14 +47 36 42 |
| HD 55677 | 440765193 | A2V | 9.4 | 10 | 07 14 31 +13 51 37 |
| HD 205905[e] | 441120034 | G1.5IV-V | 6.2 | 2 | 21 39 10 −27 18 24 |
| $\lambda$ Lep | 442871031 | B0.5IV | 4.6 | 2 | 05 19 35 −13 10 36 |
| WD1657+343 | 471015233 | DA0.9 | 15.8 | 2 | 16 58 51 +34 18 53 |

**Table 1** *continued*

**Table 1** *(continued)*

| Target Name | TIC ID | Class | T | Cadence | Coord. |
|---|---|---|---|---|---|
| | | | [mag] | min | J2000 |

NOTE—Spectral types in parenthesis are photometrically derived. References for the spectral types are the same as those specified in Gordon et al. (2022). References for the remaining spectral types is as follows: [a]Houk & Smith-Moore (1988), [b]Bohlin et al. (2011), [c]Houk (1982), [d]Cowley et al. (1969), [e]Keenan & McNeil (1989).
* Stars with names beginning with 'J' are Spitzer standards described in Reach et al. (2005) and as done their are given shortened names based on the 2MASS designation. J1757132 is 2MASS J17571324+6703409. J1802271 is 2MASS J18022716+6043356. J1732526 is 2MASS J17325264+7104431. J1805292 is 2MASS J18052927+6427520. J1808347 is 2MASS J18083474+6927286. J1812095 is 2MASS J18120957+6329423. J1743045 is 2MASS J17430448+6655015.

## 3. TESS OBSERVATIONS

To study the variability of the candidate spectrophotometric standards, we use observations from TESS spanning Sectors 1 to 40 (years 2017–2021). When possible, we utilize the 2-minute cadence data processed by the Science Processing Operations Center (SPOC) pipeline, which provides high-quality background subtraction, systematic correction and flux-dilution corrections due to the large pixel scale of TESS (Smith et al. 2020a; Clarke et al. 2020; Morris et al. 2020; Smith et al. 2020b). A few of our candidate stars were only observed by TESS in the Full Frame Images (FFIs). For these targets, we only report on their variability if MAST hosts TESS-SPOC high-level science products (Caldwell et al. 2020), since these are similarly processed by the SPOC pipeline and have corrections applied for crowding due to the large TESS pixels. These FFIs store data on the stars at a 30-minute or 10-minute cadence, depending on when the data were collected. See Table 1 for a list of those targets used in our analysis, including their TESS Input Catalog (TIC) identification and magnitude (Stassun et al. 2018). All of the data is available at MAST: DOI 10.17909/t9-tkr5-6a83.

Regardless of the data's cadence, we use the pre-search data conditioned, simple aperture photometry (PDC-SAP) photometric time series (Smith et al. 2020b) for our analysis. As an overview, the TESS pipeline that creates these light curves removes the background, performs simple aperture photometry using a fixed aperture that optimizes the signal-to-noise of the light curve, and then removes systematics by fitting Principal Component Analysis (PCA) basis vectors that represent common signals observed in nearby stars (Smith et al. 2012; Stumpe et al. 2012).

We then use the software `lightkurve` (Lightkurve Collaboration et al. 2018) to detrend and normalize the light curve. For some light curves we remove obvious systematic variations by applying a Savitzky-Golay filter (Savitzky & Golay 1964) with a window length of half of the number of data points in the sector. As a sector is ≈27 days long, we only expect to be able to unequivocally measure variability with time scales shorter than half the length of the sector. Variability longer than this time scale, unless very large in amplitude, is often mistaken for systematics and is commonly removed from the time series. While TESS data can be used to find longer-period trends, it requires very careful examination of possible systematic noise and stitching together consecutive sectors of data. For this study we restrict our analysis to repeatable variability of time scales shorter than ≈13 days in length and large-amplitude, single-occurrence variations (such as eclipses or flares).

To look for periodic variations, we used Lomb-Scargle periodograms (Lomb 1976; Lightkurve Collaboration et al. 2018) and report those with significant peaks that otherwise do not appear to be caused by systematic noise (see Section 3.1). For those with no significant variability, we provide upper limits to any variability that could be detected (see Section 3.4).

### 3.1. *Stars with Variability*

We found 15 of the JWST spectrophotometric standards stars in our sample to have statistically significant periodic variability. Only four show variability in flux larger than 1% when considering the full extent of the observed variability (minimum to maximum brightness, or peak-to-peak). For each variable star, the largest peak in the periodogram is highly significant and is at least 5 times larger than the noise level of the periodogram (Kjeldsen & Bedding 1995; Baran & Koen 2021). Figures 2 – 5 show parts of the light curve and Lomb-Scargle periodogram created from one entire

TESS sector for the 15 variable stars in our sample (two sectors for the case of HD 38949). Figure 2 highlights the four with the largest variations.

Table 2 summarizes the amplitude of the variations and their approximate period. It lists the period and amplitude of the maximum amplitude peak in the periodogram. Since most stars have more than one period of variability, the maximum amplitude in the periodogram does not capture the full change in relative flux observed in the TESS light curves. To approximate full observed peak-to-peak variability in the presence of noise, we calculate the quantity $V_{95}$, which is defined to be the difference between the maximum and minimum values of those points contained by 95.45% of the values in the light curve centered on the median. $V_{95}$ measures the envelope of all data within $\pm 2\sigma$ of the median.

When reporting the statistics we use the sectors shown in Figures 2 – 5 and bin the light curves to 6-minute bins to improve the signal-to-noise ratio in some of the dimmer stars. The displayed sectors were chosen to represent the observed variability and have the lowest observed noise. The $V_{95}$ statistic acts as a reasonable measure of the full amplitude of the observed variability for those whose amplitudes are significantly larger than the noise. For the fainter stars with low amplitudes and noisy light curves, $V_{95}$ overestimates the true extent of the observed variability. For example, for the dim variable star, J1732526 ($T_{mag}$ = 12.5), the precision on the flux (estimated from the average power in the periodogram, Kjeldsen & Bedding 1995) is 0.5%, one fifth of the $V_{95}$ statistic for this star. No single statistic will fully summarize the variability of these stars; the light curves and periodograms provide a more complete picture of the amplitude, timescale and shape of the observed periodicity.

A single TESS pixel covers more than 21 arcsec of the sky on a side and the full-width-half-max ranges from 1.13–2.76 pixels (Oelkers & Stassun 2018), making it possible for nearby sources to contaminate our light curves. As a way to quickly assess the impact of nearby sources, Table 2 includes the crowding metric calculated by the SPOC pipeline. This metric indicates the fraction of the light in the aperture that comes from the target star given the positions and amplitudes of stars in the TIC. A value near 1.0 indicates an isolated star, while lower values indicate significant crowding from neighbors. Two of our large-amplitude variables (J1732526 and J1812095) have crowding values around 0.8. The SPOC Pipeline corrects the light curve amplitudes for any dilution due to nearby stars by using this crowding value (Fausnaugh et al. 2018). As a result, the amplitudes and upper limits we report in this paper have already accounted for these neighbors.

Due to the presence of nearby stars for two of our large variables, we investigated the false positive scenario that one of the nearby stars is varying instead of the target of interest. To test this possibility, we use the code `TESS_Localize` (Higgens & Bell 2022) to determine if the location of the observed variations in the pixel time series is consistent with the position of the target star, as reported by Gaia Data Release 2 (Gaia Collaboration et al. 2018). We analyzed the large amplitude frequencies from Sector 40 data for both J1732526 and J1812095. The heat maps of per-pixel amplitudes shown in Figure 1 for J1732526 were calculated using the five largest frequencies and the two largest frequencies for J1812095 apparent in the periodogram. These per-pixel amplitudes are then fit to the TESS pixel response function (PRF) to obtain the true location of the variability. In both cases the location on the CCD of the largest amplitudes overlaps with our target star. For completeness, we analyzed all 15 variable stars similarly, despite having no bright, nearby sources. In no case did evidence emerge that a nearby source caused the variations, though for many stars with less significant variability, it was not always possible to convincingly extract and fit per-pixel variability.

### 3.2. *Reasons for Variability*

While we do not attempt to definitively explain the physical reasons for the variability we observe in these stars, it is likely the reason for the photometric variability is related to either stellar pulsations or spots.

Many of our variable stars are A dwarfs. Variability in A-type stars can occur due to a plethora of reasons, including stellar pulsations. The $\delta$ Scuti variables appear at the intersection of the instability strip and the main sequence (e.g., Petit 1987). They are the most prominent pulsators among A dwarfs, and they make up $\approx$27% of all variable A and F dwarfs (Uytterhoeven et al. 2011). They pulsate in pressure modes and mixed pressure and low-order gravity modes due to the $\kappa$ mechanism (Lee 1985), with pulsation frequencies in the range 18 min to 8 hrs (Amado et al. 2004). $\gamma$ Doradus variables also appear in a similar part of the HR diagram (e.g., Kaye et al. 1999), although they are rarer than $\delta$ Scuti stars, making up $\approx$12% of all variable A and F dwarfs. (Uytterhoeven et al. 2011). $\gamma$ Dor variables pulsate in non-radial, high-order gravity modes caused by convective blocking (Guzik et al. 2000) with pulsation periods typically on the order of one day (Grigahcène et al. 2010). Some stars, known as hybrid $\gamma$ Dor-$\delta$ Scuti

**Table 2.** Candidate spectrophotometric standards with observed variability.

| Target Name | TIC ID | Class | CROWD† | Period [days] | max Amp. [%] | $V_{95}$ [%] |
|---|---|---|---|---|---|---|
| HD 38949 | 32869782 | G1V | 0.998 | 3.798 | 0.284 | 1.17 |
| $\eta^1$ Dor | 41232189 | A0V | 1.000 | 0.249 | 0.037 | 0.18 |
| $\mu$ Col | 100589904 | O9V | 0.999 | 1.196 | 0.024 | 0.12 |
| HR 701 | 166698220 | A6V | 1.000 | 0.845 | 0.005 | 0.05 |
| HR 6514 | 198456033 | A3V | 1.000 | 0.054 | 0.058 | 0.42 |
| J1808347 | 219114641 | A3V | 0.991 | 0.026 | 0.419 | 1.65 |
| HD 163466 | 219820925 | A6V | 1.000 | 0.101 | 0.064 | 0.17 |
| J1732526 | 219897252 | A3V | 0.831 | 0.020 | 0.178 | 1.40 |
| J1812095 | 233095291 | A3V | 0.780 | 2.442 | 0.396 | 1.57 |
| HR 5467 | 298165335 | A1V | 1.000 | 0.995 | 0.004 | 0.05 |
| $\delta$ UMi | 383553764 | A1V | 1.000 | 0.761 | 0.004 | 0.04 |
| HR 7018 | 383676357 | A0V | 0.996 | 2.547 | 0.029 | 0.13 |
| HD 55677 | 440765193 | A4V | 0.984 | 0.145 | 0.029 | 0.24 |
| HD 205905 | 441120034 | G2V | 0.999 | 9.986 | 0.068 | 0.26 |
| $\lambda$ Lep | 442871031 | B0.5V | 1.000 | 1.260 | 0.148 | 0.35 |

NOTE—The column Period gives the period of the largest amplitude peak (max Amp.) seen in the periodogram. $V_{95}$ is the peak-to peak range encompassing 95.45% of the binned observed relative fluxes. Errors on the max Amp. value are less than 0.002% with the exception being the 'J' stars ($T_{mag} \geq 11$) whose errors are near 0.01%.
†CROWD comes from the CROWDSAP estimate from the TESS SPOC pipeline and is the fraction of flux from the target in the extracted aperture.

stars, exhibit both $\gamma$ Dor and $\delta$ Scuti pulsations (Grigahcène et al. 2010). These hybrid pulsators account for an additional ≈23% of all variability found in A and F dwarfs. In our sample we find evidence of all three types of the above pulsators at varying amplitudes.

Other than pulsations, binarity and rotational modulation due to spots can also cause variations in A stars. In our sample, we do not find evidence of short-period, eclipsing binarity which is expected since these usually have large flux variations that would have been seen in previous observations. Regarding rotation, Balona (2013, 2017) claim to have found spots in more than 50% of A stars in the Kepler data, suggesting that modulation due to surface rotation is more commonly observed than previously thought. However, the origin of spots in A and B stars is currently under debate, as these stars do not have a significant surface convective zone, which is usually associated with surface spots. The presence of a fossil magnetic field (Parker 1955) and the creation of a magnetic field caused by a dynamo effect in mass motions that occur in convective layers (Charbonneau 2014) are two of the contending ideas for the creation of spots in hotter main sequence stars. In our sample, we find signatures that suggest the presence of spots in several objects: HD 38949, J1812095, $\lambda$ Lep, $\eta^1$ Dor, and HR 7018.

### 3.3. *Large Amplitude Variable Stars*

In this section we discuss in more detail the size and astrophysics for the variability of the six stars with the largest changes in brightness that we measured in the TESS data from our target list. Each of these stars show a $V_{95} \geq 0.35\%$. In these cases, the time scale and amplitude of the variations could impact high precision spectrophotometric calibrations, and their variability should be considered before using them as a standard star. The remaining nine stars have small enough amplitudes that at least for JWST they will not significantly impact the calibrations.

Three of the large-amplitude variable stars are A dwarfs from the Reach et al. (2005) Spitzer calibration. The amplitudes we see here were likely below the level of detection for Spitzer. For comparison, Krick et al. (2021) measured the IRAC fluxes in dozens to thousands of observations for most of our variable stars and reported standard deviations between 0.7% and 2.8%

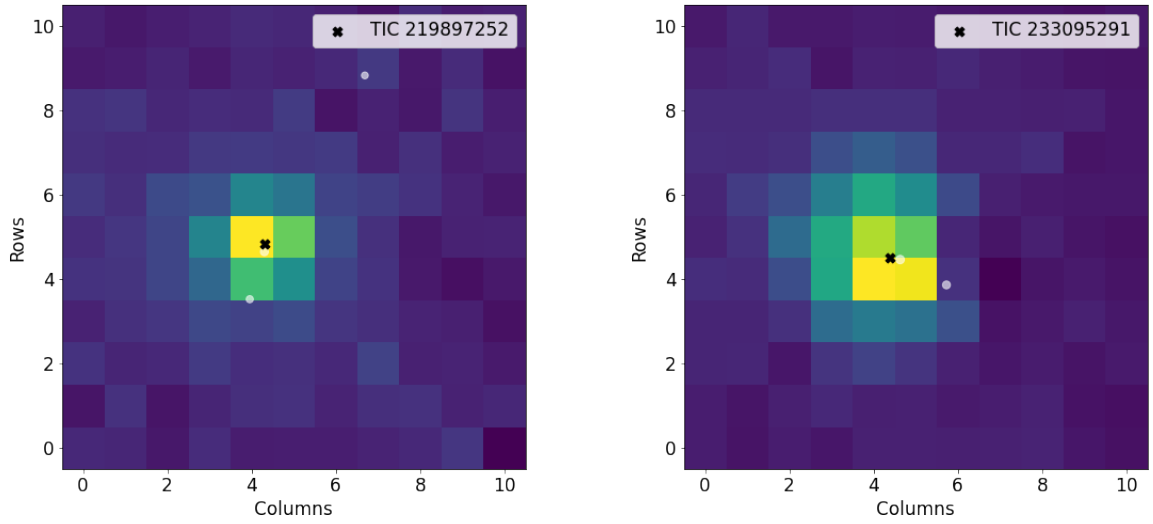


**Figure 1.** Heat maps of the fitted amplitudes for each 21 arc second pixels at the observed periods across the pixels downloaded from TESS in Sector 40 for this target (generated by `TESS_Localize` Higgens & Bell 2022.) TIC 219897252 (J1732526) is on the left and TIC 233095291 (J1812095) is on the right. The grey circles represent known Gaia Data Release 2 sources with $T_{mag} > 15$, approximately three magnitudes dimmer than the target stars. The black 'x' represents the best fit between the heat map and the TESS PRF. In both cases the best fit location overlaps the Gaia location of our target at the center of the TESS pixels, indicating that the variability comes from the targeted source.

for the 3.6 $\mu m$ band. This observed scatter is approximately four times larger than the variability we report here.

#### 3.3.1. *HD 38949 (TIC 32869782)*

This G dwarf ($T_{mag} = 7.3$) varies with a peak-to-peak amplitude of 1.2% (Figure 2, top panel). TESS observed HD 38949 in Sectors 6, 32, and 33. The power spectrum is complex and shows a 7.9-day peak along with peaks at both a half and quarter of that period. This quasi-periodic, oscillatory behavior is consistent with a combination of stellar rotation at a 7.9-day period and migrating star spots on the surface due to strong magnetic activity (Santos et al. 2021). HD 38949 is also an x-ray source, as revealed by the Swift Observatory (Evans et al. 2020, 2019), which supports a picture of active spots and flares. Due to these properties, the JWST calibration team has already removed this star from the list of standards (Gordon et al. 2022).

It is also noteworthy that HD 38949 is listed in the Hubble Space Telescope Calspec database[2] (Bohlin et al. 2014) as a star with complete STIS coverage that could be used to support flux calibrations of other observatories.

[2] https://www.stsci.edu/hst/instrumentation/reference-data-for-calibration-and-tools/astronomical-catalogs/calspec

#### 3.3.2. *J1808347 (TIC 219114641)*

This A dwarf ($T_{mag} = 11.9$) shows a rich set of peaks in its periodogram that produce a peak-to-peak amplitude of 1.65% (Figure 2, second panel). These variations compromise its ability to act as a spectrophotometric standard. The periods range from 0.5 to 1.0 hours, with the strongest mode at 0.6 hours. The high-frequency variations are caused by $\delta$ Scuti pulsations. The variability is difficult to see in the 30-minute TESS data taken during the first year of TESS observations; however, they are more apparent in the 2-minute cadence data from Sectors 40 and 41. This star will be observed again by TESS in Sectors 47–55.

#### 3.3.3. *J1732526 (TIC 219897252)*

J1732526 is an A dwarf ($T_{mag} = 12.5$) that behaves much like J1808347; it is multiperiodic, with its strongest mode having a period of 0.5 hours, suggesting most of the variability arises from $\delta$ Scuti pulsations (Figure 2, third panel). Its light curve has a peak-to-peak amplitude of roughly 1.4%, limiting its value as a spectrophotometric standard. However, in this case, this statistic is somewhat inflated by the inherent noise

of this dim object. The combined amplitudes of the largest peaks point to a peak-to-peak variation closer to 1%. In addition to the roughly 0.5-hour pulsation modes, the light curve also shows a longer-period component (roughly 2.5 days). This latter component could arise from rotation, or it could indicate that J1732526 is a hybrid $\delta$ Scuti ($p$-mode) – $\gamma$ Doradus ($g$-mode) pulsator. TESS observed this star at a 2-minute cadence in Sectors 40 and 41 and is planning to observe it again in Sectors 48–55.

#### 3.3.4. *J1812095 (TIC 233095291)*

This A dwarf ($T_{mag} = 11.6$) shows consistent oscillations with periods of 1–3 days and peak-to-peak changes in the flux greater than 1.5% in the TESS bandpass (Figure 2, bottom panel). The light curve and periodogram show significant (though somewhat variable in amplitude) variations at a period of 2.44 days, with a secondary peak at exactly half that period, which indicates rotational modulation due to spots. The periodogram shows no evidence for short-period peaks (i.e., for periods of an hour or less). TESS observed this star in Sectors 14–26 at a 30-minute cadence, and at a 2-minute cadence in Sector 40. The variability is approximately the same across all sectors. The large peak-to-peak variability on long time scales may make this target unsuitable for high-precision spectrophotometric calibration.

#### 3.3.5. *HR 6514 (TIC 198456033)*

The periodogram of this bright A dwarf ($T_{mag} = 6.4$) shows a complex set of peaks with periods between roughly 0.5 and 2.0 hours, with up to 0.42% peak-to-peak variability (Figure 3, top panel). The strongest mode has a period of 1.3 hours. The periodicity is too fast to arise from stellar rotation and thus likely arises from short-period, $\delta$ Scuti ($p$-mode) pulsations. TESS observed this star in Sectors 14–26 and 40–41, and is expected to observe it again in Sectors 47–55. In the present data, the variability is consistent in amplitude from one sector to the next.

#### 3.3.6. *$\lambda$ Lep (TIC 442871031)*

This B9.5 dwarf ($T_{mag} = 4.6$) varies with a coherent period of 1.26 days and multiple, exact harmonics of this base period, which suggests that the variation is due to spots on the stellar surface. The peak-to-peak amplitude is greater than 0.3% (Figure 3, bottom panel). TESS observed this star in two sectors: 5 and 32. In both sectors the variability was similar in amplitude and shape. $\lambda$ Lep is one of the hot B dwarfs under consideration for use as standards starting in JWST Cycle 2 (Gordon et al. 2022).

### 3.4. *Not Observed to Vary*

We find no significant variability in 22 of the 37 stars we examined with existing TESS data. Figure 6 displays the light curves and periodograms for three well-known calibration stars with no significantly detected variability. We note that TESS commonly has large-amplitude systematic noise in its light curves at long periods, including noise at periods of 2 weeks due to the orbit of the spacecraft and near 1 day due to scattered light from the rotation of the Earth (Luger et al. 2019). Our sample of variable stars does not include those stars that only showed evidence of these types of systematic noise.

For those cases with no significant variability, we provide two statistics to better understand the upper limits of variability that could exist undetected in the TESS data in Table 3. The photometric precision achieved by the TESS data is mostly driven by the brightness of the star, though in some cases systematic noise is playing a part. The quantity $A^{max}_{<1d}$ is the maximum amplitude peak in the periodogram seen at periods less than 1 day. This statistic can serve as measure of the upper limit on consistent, short-period variability. $V_{99.7\%}$ can be interpreted as the largest peak-to-peak variation on time scales longer than 30-minutes that could be present in the data without detection. It is calculated by binning the light curve to a 30-minute cadence and reporting the difference between the minimum and maximum relative flux for those points that lie within 99.7% of the median observed flux. If the data are predominantly Gaussian noise, this value is approximately six times the size of the standard deviation of the light curve. For both of these statistics we report the sector that gives the smallest value, as some TESS sectors are noisier than others depending on scattered light from the Earth and Moon.

TESS is able to provide limits to changes in brightness below 1% for all but six stars, all of which are dimmer than 12.9 mag in the TESS band. For all but our dimmest star, TESS sees no evidence of coherent, periodic variability with amplitudes larger than 0.2% for periods shorter than 1 day. Thus, TESS can still confirm the suitability as flux standards of many of the faintest sources in our sample.

## 4. CONCLUSIONS

The high-cadence, all-sky photometric survey of bright stars produced by TESS is a useful resource to vet potential spectrophotometric calibration stars for variability on time scales of a few minutes to a couple of weeks. The precise relative photometry, month-long stares, and fast cadence provided by TESS is a significant improvement over previous efforts to vet these stars

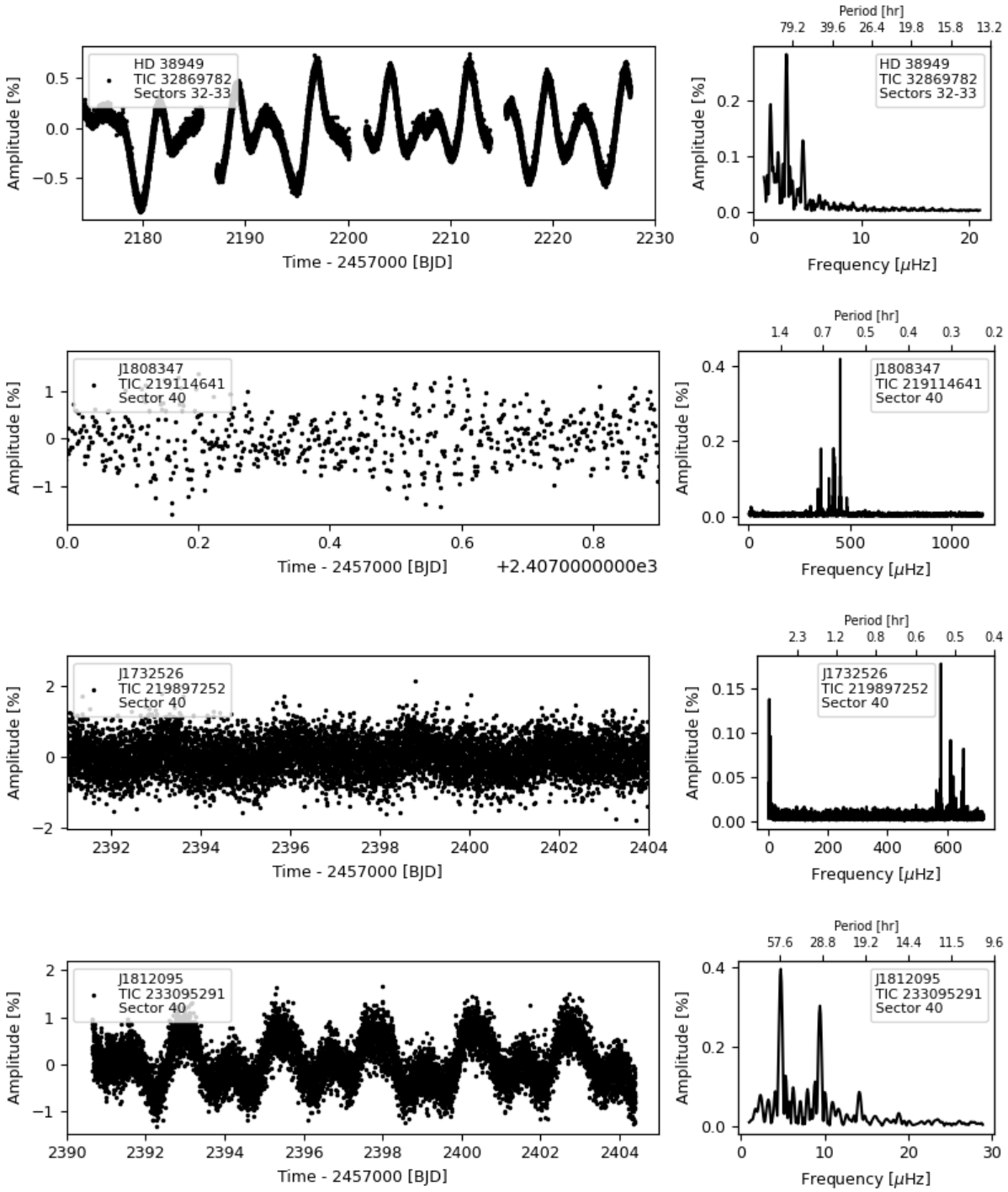


**Figure 2.** Light curve (left) and periodogram (right) of stars with peak to peak detected variability larger than approximately half a percent. The TESS sector(s) used to generate both are labeled on each plot.

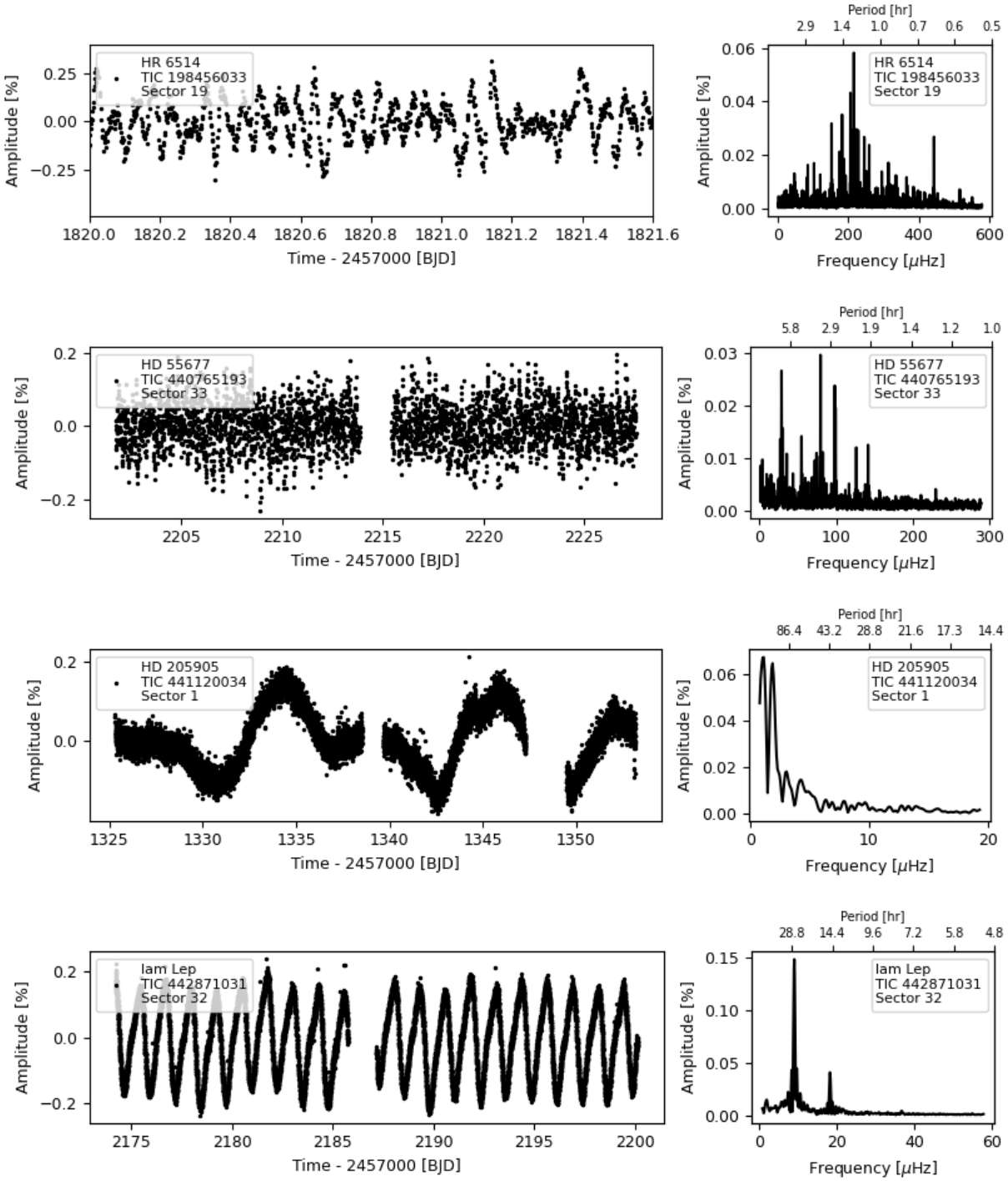


**Figure 3.** Light curve (left) and periodogram (right) of stars with significant detected variability. The TESS sector used to generate both are labeled on each plot.

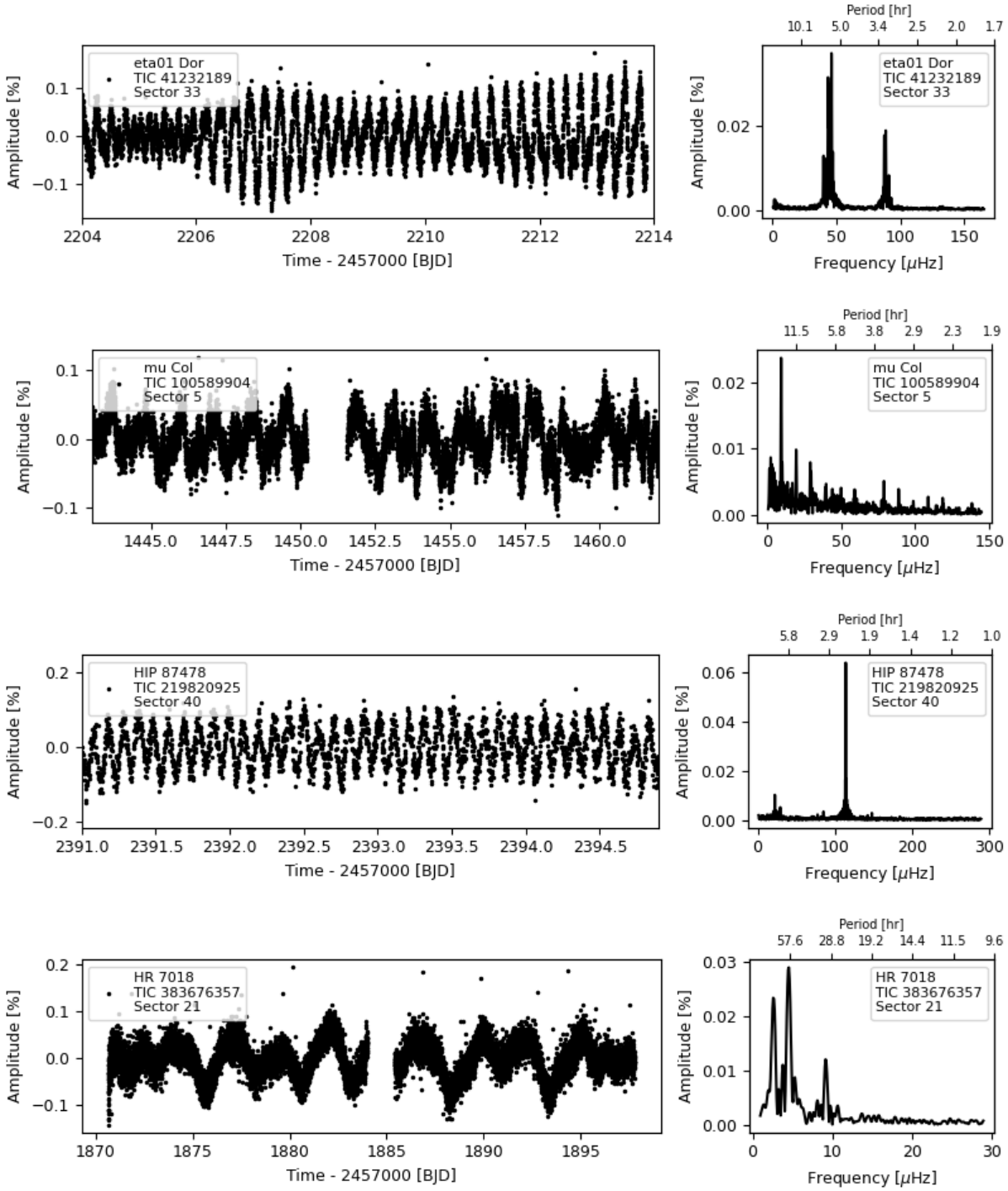


**Figure 4.** Light curve (left) and periodogram (right) of stars with significant detected variability. The TESS sector used to generate both are labeled on each plot.

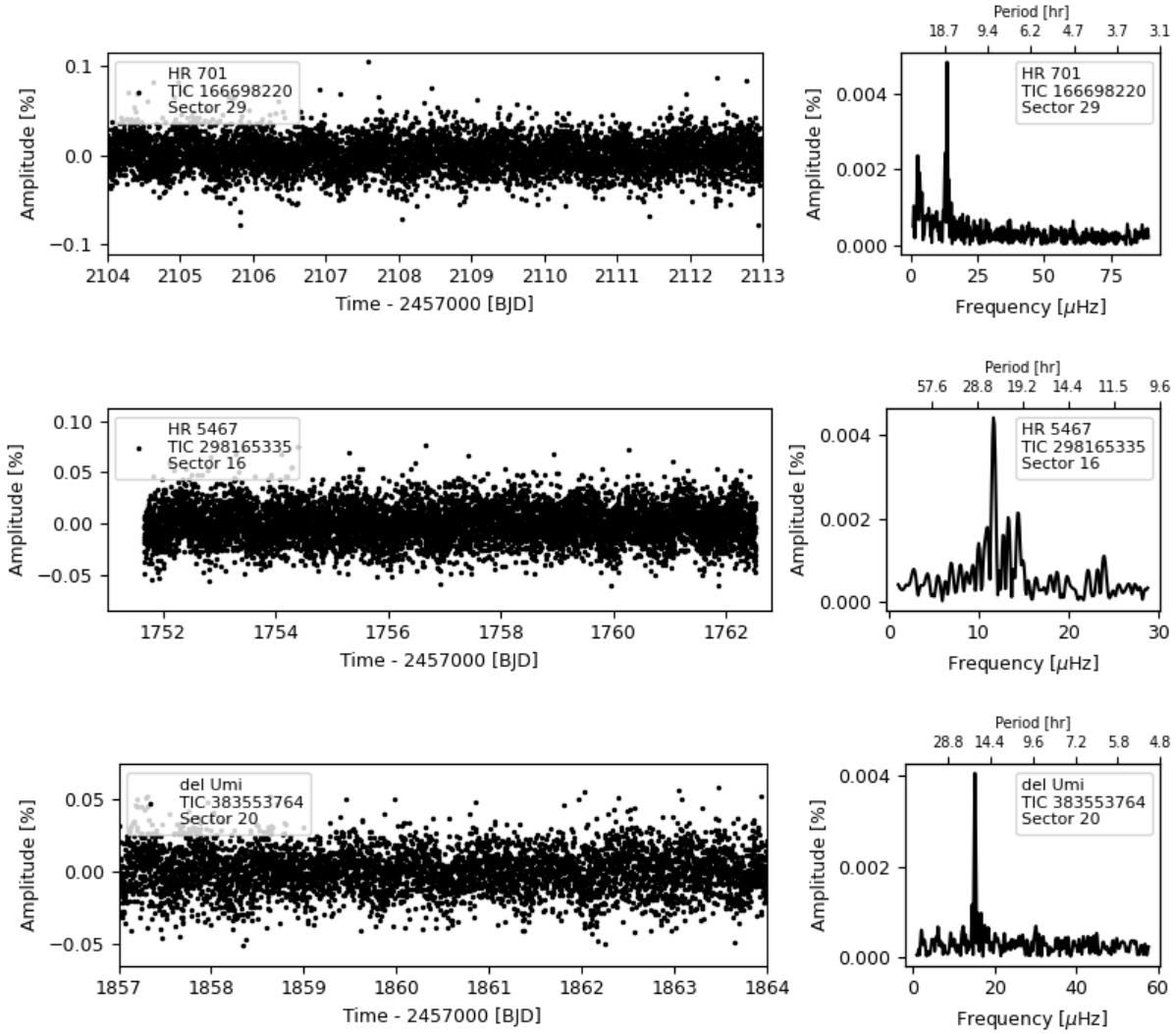


**Figure 5.** Light curve (left) and periodogram (right) of stars with significant detected variability. The TESS sector(s) used to generate both are labeled on each plot.

**Table 3.** Upper limits on variability for those with no significant variations.

| Name | TIC ID | Class | $T$ [mag] | CROWD† | $A_{<1d}^{max}$ [%] | $V_{99.7}$ [%] |
|---|---|---|---|---|---|---|
| GSPC P330-E | 8591766 | G2V | 12.4 | 0.891 | 0.021 | 0.76 |
| 16 Cyg B* | 27533327 | G3V | 5.6 | 0.630 | 0.017 | 0.21 |
| HD 6538 | 39464221 | G1V | 5.9 | 0.998 | 0.003 | 0.09 |
| 10 Lac | 128692445 | O9V | 5.1 | 0.993 | 0.007 | 0.23 |
| HD 37962 | 140282069 | G2V | 7.2 | 1.000 | 0.002 | 0.09 |
| WD 1057+719 | 147921014 | DA1.2 | 15.1 | 0.919 | 0.148 | 6.05 |
| GD153 | 149505899 | DA1 | 13.7 | 0.987 | 0.062 | 2.44 |
| HD 116405 | 165370459 | B9V | 8.4 | 0.969 | 0.003 | 0.10 |
| HD 101452 | 181240911 | A9mIV | 7.3 | 0.993 | 0.003 | 0.09 |
| J1757132 | 219094190 | A3V | 11.6 | 0.963 | 0.010 | 0.37 |
| GSPC P041C | 219015049 | G0 | 11.5 | 0.995 | 0.011 | 0.44 |
| BD+60 1753 | 219752116 | A1V | 9.7 | 0.992 | 0.006 | 0.17 |
| HD 180609 | 229945862 | A3V | 9.3 | 0.984 | 0.005 | 0.13 |
| HD 115169 | 229980646 | G2V | 8.7 | 0.984 | 0.003 | 0.11 |
| J1802271 | 233067231 | A3V | 12.0 | 0.963 | 0.023 | 0.82 |
| J1805292 | 233075513 | A1V | 12.2 | 0.965 | 0.014 | 0.49 |
| J1743045 | 233205654 | A5V | 13.3 | 0.986 | 0.032 | 1.32 |
| GD71 | 247923021 | DA1 | 13.4 | 0.788 | 0.055 | 1.90 |
| G191-B2B | 327587572 | DA0 | 12.2 | 0.903 | 0.021 | 0.74 |
| HD 167060 | 365653206 | G2V | 8.4 | 0.994 | 0.002 | 0.09 |
| GSPC P177-D | 417544924 | G2V | 12.9 | 0.942 | 0.028 | 1.00 |
| WD1657+343 | 471015233 | DA1 | 15.8 | 0.631 | 1.289 | 37.88 |

Note—*16 Cyg B is a known solar-type variable with low-amplitude modes (smaller than the limits reported here) at periods near 8 minutes (see Metcalfe et al. 2012). $A_{<1d}^{max}$ is the maximum amplitude peak seen in the periodogram less than 1 day. $V_{99.7}$ is peak to peak flux change of those relative fluxes that lie within 99.7% of the median flux.
†CROWD comes from the CROWDSAP estimate from the TESS SPOC pipeline and is the fraction of the flux that comes from the target star in the extracted aperture, as opposed to nearby sources in the TIC.

and has revealed peak-to-peak changes in flux as large as 1.4% for four of the JWST candidate calibrators. Another 11 show lower amplitude variability. This variability appears to arise from either stellar pulsations or stellar spots rotating in and out of view. At the same time, relative photometry from TESS has set upper limits on optical to near-infrared variability for most of the candidate standard stars at a level well below that needed to achieve the spectrophotometric requirements for JWST. Identifying those with known issues provides the JWST calibration team with information necessary to pick those stars with the highest likelihood of accurate calibrations in the least amount of observing time. This work has already led to revisions of the JWST spectrophotometric calibration star list, see Gordon et al. (2022).

Some of the stars vetted in this paper are the same stars that were used to calibrate telescopes such as Spitzer (Reach et al. 2005) and Hubble (Bohlin et al. 2011), and some may be used to calibrate future space and ground-based telescopes. Because TESS is an ongoing all-sky survey, in the future TESS will serendipitously continue to monitor many of the JWST spectrophotometric calibration stars. This monitoring by TESS will reveal if the star varies photometrically in new or unexpected ways. Some of these observations may even be contemporaneous with the JWST calibration observations, as both missions plan to be operating

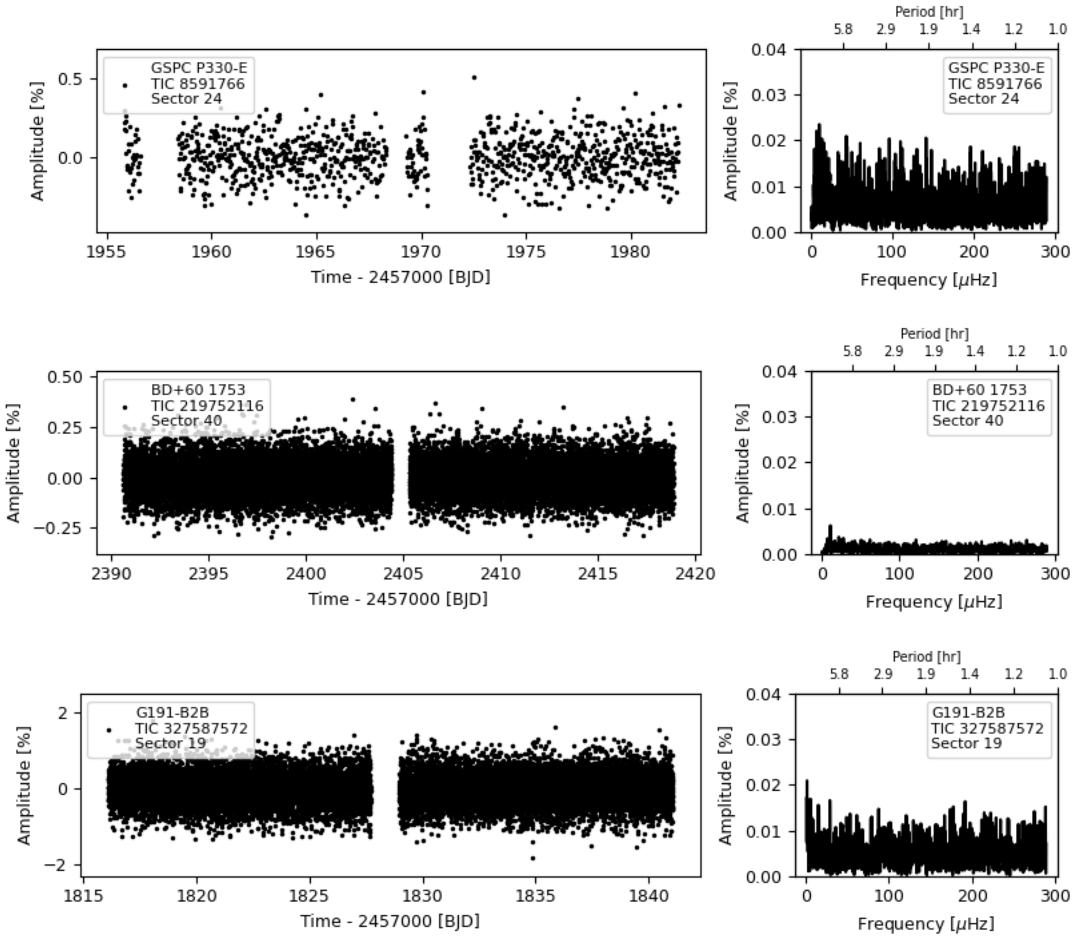


**Figure 6.** Light curves and Lomb-Scargle periodograms of three common calibration stars that show no significant, coherent variability in the TESS light curves.

at the same time. This work provides further evidence that small NASA missions like TESS can provide crucial supporting observations which enable larger missions like JWST to accomplish their science goals.

This paper includes data collected by the TESS mission. Funding for the TESS mission is provided by NASA's Science Mission Directorate. We thank the STScI internship program and JWST for providing funding for MK. JJH acknowledges financial support through NASA Award 80NSSC20K0592. This research has made use of the VizieR catalogue access tool, CDS, Strasbourg, France (DOI: 10.26093/cds/vizier). The original description of the VizieR service was published in A&AS 143, 23. This research has been made possible by the MAST archive for access to the TESS light curves, target pixel files, and TESS Input Catalog.

*Facilities:* TESS, JWST, MAST

*Software:* astropy (Astropy Collaboration et al. 2013, 2018), lightkurve (Lightkurve Collaboration et al. 2018), TESS_Localize (Higgens & Bell 2022)

## REFERENCES


Amado, P. J., Moya, A., Suárez, J. C., et al. 2004, MNRAS, 352, L11, doi: 10.1111/j.1365-2966.2004.08116.x

Astropy Collaboration, Robitaille, T. P., Tollerud, E. J., et al. 2013, A&A, 558, A33, doi: 10.1051/0004-6361/201322068

Astropy Collaboration, Price-Whelan, A. M., Sipőcz, B. M., et al. 2018, AJ, 156, 123, doi: 10.3847/1538-3881/aabc4f

Auvergne, M., Bodin, P., Boisnard, L., et al. 2009, A&A, 506, 411, doi: 10.1051/0004-6361/200810860

Balona, L. A. 2013, MNRAS, 431, 2240, doi: 10.1093/mnras/stt322

—. 2017, MNRAS, 467, 1830, doi: 10.1093/mnras/stx265

Baran, A. S., & Koen, C. 2021, AcA, 71, 113, doi: 10.32023/0001-5237/71.2.3

Bohlin, R. C., Gordon, K. D., & Tremblay, P. E. 2014, PASP, 126, 711, doi: 10.1086/677655

Bohlin, R. C., Gordon, K. D., Rieke, G. H., et al. 2011, AJ, 141, 173, doi: 10.1088/0004-6256/141/5/173

Boyajian, T. S., LaCourse, D. M., Rappaport, S. A., et al. 2016, MNRAS, 457, 3988, doi: 10.1093/mnras/stw218

Breger, M. 1979, PASP, 91, 5, doi: 10.1086/130433

Caldwell, D. A., Tenenbaum, P., Twicken, J. D., et al. 2020, Research Notes of the American Astronomical Society, 4, 201, doi: 10.3847/2515-5172/abc9b3

Charbonneau, P. 2014, ARA&A, 52, 251, doi: 10.1146/annurev-astro-081913-040012

Clarke, B. D., Caldwell, D. A., Quintana, E. V., et al. 2020, Kepler Data Processing Handbook: Pixel Level Calibrations, Kepler Science Document KSCI-19081-003

Cohen, M., Walker, R. G., & Witteborn, F. C. 1992, AJ, 104, 2030, doi: 10.1086/116379

Cotton, D. V., Bailey, J., De Horta, A. Y., Norris, B. R. M., & Lomax, J. R. 2020, Research Notes of the American Astronomical Society, 4, 39, doi: 10.3847/2515-5172/ab7f2f

Cowley, A., Cowley, C., Jaschek, M., & Jaschek, C. 1969, AJ, 74, 375, doi: 10.1086/110819

Evans, P. A., Page, K. L., Osborne, J. P., et al. 2019, VizieR Online Data Catalog, IX/58

—. 2020, ApJS, 247, 54, doi: 10.3847/1538-4365/ab7db9

Fausnaugh, M. M., Caldwell, D. A., Jenkins, J. A., Smith, J. C., & Vanderspek, R. 2018, TESS Data Release Notes

Gaia Collaboration, Brown, A. G. A., Vallenari, A., et al. 2018, A&A, 616, A1, doi: 10.1051/0004-6361/201833051

Gardner, J. P., Mather, J. C., Clampin, M., et al. 2006, SSRv, 123, 485, doi: 10.1007/s11214-006-8315-7

Gordon, K., Bohlin, R., Boyer, M., et al. 2022, in prep

Grigahcène, A., Antoci, V., Balona, L., et al. 2010, ApJL, 713, L192, doi: 10.1088/2041-8205/713/2/L192

Guidry, J. A., Vanderbosch, Z. P., Hermes, J. J., et al. 2021, ApJ, 912, 125, doi: 10.3847/1538-4357/abee68

Guzik, J. A., Kaye, A. B., Bradley, P. A., Cox, A. N., & Neuforge, C. 2000, ApJL, 542, L57, doi: 10.1086/312908

Hermes, J. J., Gänsicke, B. T., Gentile Fusillo, N. P., et al. 2017, MNRAS, 468, 1946, doi: 10.1093/mnras/stx567

Higgens, M., & Bell, K. 2022, in prep. github.com/Higgins00/TESS-Localize

Houk, N. 1982, Michigan Catalogue of Two-dimensional Spectral Types for the HD stars. Volume_3. Declinations -40_f0 to -26_f0.

Houk, N., & Smith-Moore, M. 1988, Michigan Catalogue of Two-dimensional Spectral Types for the HD Stars. Volume 4, Declinations -26°.0 to -12°.0., Vol. 4

JWST User Documentation. 2016, https://jwst-docs.stsci.edu/

Kalirai, J. 2018, Contemporary Physics, 59, 251, doi: 10.1080/00107514.2018.1467648

Kaye, A. B., Handler, G., Krisciunas, K., Poretti, E., & Zerbi, F. M. 1999, PASP, 111, 840, doi: 10.1086/316399

Keenan, P. C., & McNeil, R. C. 1989, ApJS, 71, 245, doi: 10.1086/191373

Kilic, M., Gianninas, A., Bell, K. J., et al. 2015, ApJL, 814, L31, doi: 10.1088/2041-8205/814/2/L31

Kjeldsen, H., & Bedding, T. R. 1995, A&A, 293, 87. https://arxiv.org/abs/astro-ph/9403015

Koch, D. G., Borucki, W. J., Basri, G., et al. 2010, ApJL, 713, L79, doi: 10.1088/2041-8205/713/2/L79

Krick, J. E., Lowrance, P., Carey, S., et al. 2021, AJ, 161, 177, doi: 10.3847/1538-3881/abe390

Lee, U. 1985, PASJ, 37, 279

Lightkurve Collaboration, Cardoso, J. V. d. M., Hedges, C., et al. 2018, Lightkurve: Kepler and TESS time series analysis in Python, Astrophysics Source Code Library. http://ascl.net/1812.013

Lomb, N. R. 1976, Ap&SS, 39, 447, doi: 10.1007/BF00648343

Luger, R., Bedell, M., Vanderspek, R., & Burke, C. J. 2019, arXiv e-prints, arXiv:1903.12182. https://arxiv.org/abs/1903.12182

Marinoni, S., Pancino, E., Altavilla, G., et al. 2016, MNRAS, 462, 3616, doi: 10.1093/mnras/stw1886

McQuillan, A., Mazeh, T., & Aigrain, S. 2014, ApJS, 211, 24, doi: 10.1088/0067-0049/211/2/24

Metcalfe, T. S., Chaplin, W. J., Appourchaux, T., et al. 2012, ApJL, 748, L10, doi: 10.1088/2041-8205/748/1/L10

Montargès, M., Cannon, E., Lagadec, E., et al. 2021, Nature, 594, 365, doi: 10.1038/s41586-021-03546-8

Morris, R. L., Twicken, J. D., Smith, J. C., et al. 2020, Kepler Data Processing Handbook: Photometric Analysis, Kepler Science Document KSCI-19081-003
Oelkers, R. J., & Stassun, K. G. 2018, AJ, 156, 132, doi: 10.3847/1538-3881/aad68e
Parker, E. N. 1955, ApJ, 121, 491, doi: 10.1086/146010
Petit, M. 1987, Variable stars
Price, S. D., Sloan, G. C., & Kraemer, K. E. 2002, ApJL, 565, L55, doi: 10.1086/339055
Provencal, J. L., Montgomery, M. H., Kanaan, A., et al. 2009, ApJ, 693, 564, doi: 10.1088/0004-637X/693/1/564
Prša, A., Batalha, N., Slawson, R. W., et al. 2011, AJ, 141, 83, doi: 10.1088/0004-6256/141/3/83
Reach, W. T., Megeath, S. T., Cohen, M., et al. 2005, PASP, 117, 978, doi: 10.1086/432670
Ricker, G. R., Winn, J. N., Vanderspek, R., et al. 2015, Journal of Astronomical Telescopes, Instruments, and Systems, 1, 014003, doi: 10.1117/1.JATIS.1.1.014003
Santos, A. R. G., Breton, S. N., Mathur, S., & García, R. A. 2021, ApJS, 255, 17, doi: 10.3847/1538-4365/ac033f
Savitzky, A., & Golay, M. J. E. 1964, Analytical Chemistry, 36, 1627
Scaringi, S., de Martino, D., Buckley, D. A. H., et al. 2021, Nature Astronomy, doi: 10.1038/s41550-021-01494-x
Sloan, G. C., Herter, T. L., Charmandaris, V., et al. 2015, AJ, 149, 11, doi: 10.1088/0004-6256/149/1/11
Smith, J. C., Morris, R. L., Jenkins, J. M., et al. 2020a, Kepler Data Processing Handbook: Finding Optimal Apertures in Kepler Data, Kepler Science Document KSCI-19081-003
Smith, J. C., Stumpe, M. C., Van Cleve, J. E., et al. 2012, PASP, 124, 1000, doi: 10.1086/667697
Smith, J. C., Stumpe, M. C., Jenkins, J. M., et al. 2020b, Kepler Data Processing Handbook: Presearch Data Conditioning, Kepler Science Document KSCI-19081-003
Stassun, K. G., Oelkers, R. J., Pepper, J., et al. 2018, AJ, 156, 102, doi: 10.3847/1538-3881/aad050
Stumpe, M. C., Smith, J. C., Van Cleve, J. E., et al. 2012, PASP, 124, 985, doi: 10.1086/667698
Thompson, S. E., Coughlin, J. L., Hoffman, K., et al. 2018, ApJS, 235, 38, doi: 10.3847/1538-4365/aab4f9
Uytterhoeven, K., Moya, A., Grigahcène, A., et al. 2011, A&A, 534, A125, doi: 10.1051/0004-6361/201117368
Vanderburg, A., Johnson, J. A., Rappaport, S., et al. 2015, Nature, 526, 546, doi: 10.1038/nature15527